Computational study of a novel valveless design of a macroscale piston pump

T. Machů^{a,*}, F. Pochylý^{a}, J. Šulc^{b}

^{a}*Faculty of Mechanical Engineering, Brno University of Technology, Technická 2896/2, 616 69 Brno, Czech Republic*
^{b}*Faculty of Civil Engineering, Brno University of Technology, Veveří 331/95, 602 00 Brno, Czech Republic*

Abstract

This paper deals with a novel valveless piston pump, which is using modified Venturi diodes as a replacement for common check valves. The pump characteristic was obtained from CFD simulations in ANSYS Fluent software. The simulations were carried out on a simplified 2D geometry model of the pump. The dependencies of the volumetric efficiency of the pump on parameters of piston motion (frequency and amplitude) and backpressure are the results of the simulations. The principle of the pump is based on different rates of dissipation in the discharge and the suction diode. The paper also presents a qualitative analysis of dissipation function for turbulent flow, which provides further insight into the principle of valveless pumping.
© 2019 University of West Bohemia. All rights reserved.

1. Introduction

Check valves are integral parts of displacement pumps which use a piston or a membrane for the transport of fluid. Valves secure proper fluid flow through a pump. At the same time, they are considered to be the most unreliable parts of said pumps. Valves can be also clogged if a fluid mixture is being pumped. These liabilities are the reason why principles of valveless pumping have been studied.

Valveless pumping can be achieved via several methods. The most common approach is the use of fluidic diodes. Fluidic diodes are components with different hydrodynamic properties dependent on the direction of flow. These diodes are used as a replacement for common check valves. Various designs of fluidic diodes are used in microfluidic pumps. The first micropump with fluidic diodes used diffuser/nozzle elements, also called Venturi diodes [11]. Many variants of Venturi diodes are used in micropumps nowadays, e. g., [3, 4, 8]. A Tesla valve is another type of fluidic diode which is used in micropumps [1, 2, 5], even though it was invented by N. Tesla for macro scale usage [14]. The last type of commonly used fluidic diode is a vortex diode, which is applied more in macro scale than in micro scale [6, 7, 15]. Pumps with vortex diodes are generally driven by pressure/vacuum of a gas in a tank instead of a piston or a diaphragm [7, 15]. The reason is the need to achieve very low frequency of the change in the direction of flow at which the diodes have the best performance [13].

Impedance pumps have a very simple design. They consist of only two kinds of tubes, the tube for delivering liquid is more rigid than the tube for generating the fluid motion. The generation of fluid motion is secured by the so-called Liebau effect, when the less rigid tube is periodically pressed. This principle of pumping can be used for both open and closed loops and also for macro and micro scale pumping [9, 10, 16].

Another principle of valveless pumping was presented in [12]. The pump was designed for macro scale pumping of hazardous liquids and uses the Coanda effect to generate a travelling wave which travels through several stages of the pump. Each stage has a displacement chamber connected to a system that is periodically pressurising/de-pressurising the chamber. At one time odd chambers are pressurised and even chambers are de-pressurised and vice versa. In that way, the generated wave is travelling from one stage to another towards the outlet of the pump.

In general, valveless pumps can be divided into two groups: micro and macro scale pumps. Micro scale pumps are commonly used in various microfluidic devices such as chemical analysis systems, microdosage systems, etc. Macro scale pumps are used mainly for the pumping of hazardous fluids where the demands on reliability are much higher than the demands on efficiency. This work presents a mathematical model of a valveless piston pump and the results of CFD analysis of a novel valveless piston pump for macro scale pumping.

2. Pump geometry

The pump geometry (Fig. 1) consists of a piston chamber, two diodes and an outlet piping. The piston chamber is perpendicularly connected to the piping. The diodes are placed close to the piston chamber inside the suction/discharge piping. The diodes are fitted with obstacles which should cause the creation of vortices when flow rate occurs in the desired direction. Vortices created near the obstacles increase the hydraulic losses which results in a lower flow rate through the diode and a higher volumetric efficiency of the pump. The suction and discharge piping was extended so that the outlet boundary conditions do not influence the flow inside the pump.
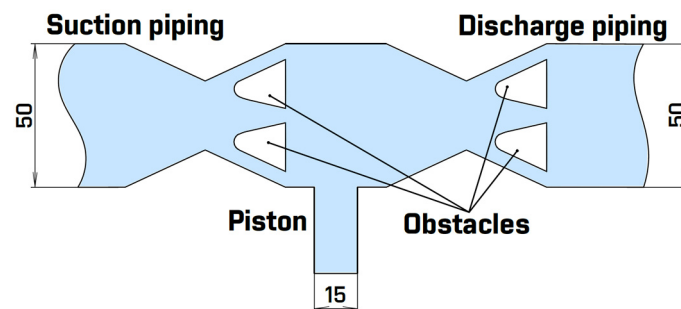
Fig. 1. Pump geometry, dimensions are in millimetres

3. CFD preprocessing

In order to obtain the characteristics of the pump, CFD calculations were carried out. Simplified 2D geometry of the pump was used for all calculations. Computational mesh (Fig. 2) was created in ANSYS ICEM CFD. The computational domain consisted of approximately 70 000 hexahedral cells.
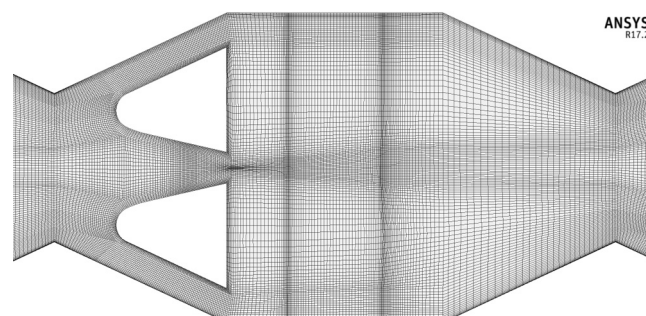
Fig. 2. Part of the 2D domain mesh
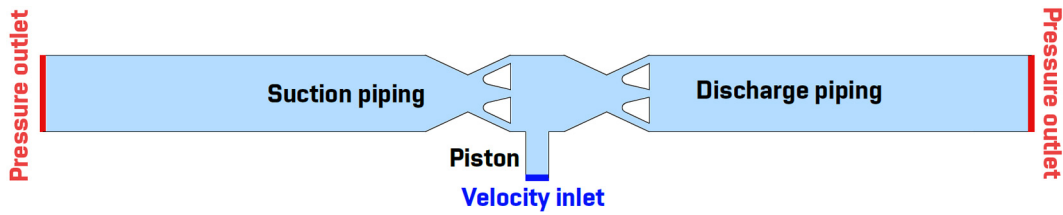
Fig. 3. The entire computational domain with boundary conditions

Outlet boundary conditions were set at the end of the suction and the discharge piping (Fig. 3). The suction and discharge piping was extended so that the outlet boundary conditions do not influence the flow inside the pump.

Another simplification was made with the motion of the piston, which was simulated by a time-dependent inlet boundary condition placed at the beginning of the piston part of the pump. The inlet boundary condition was controlled by the following function:

$$v_{\text{inlet}} = 2\pi f A \cos(2\pi f t), \tag{1}$$

where f is the frequency of the piston movement, A is the amplitude of the piston movement and t is the time of the calculation. The settings of all calculated cases are listed in Table 1.

Table 1. Settings of all calculated cases

Turbulence model	Realizable k-ε
Near-wall treatment	Non-equilibrium wall function
Pressure-velocity coupling	SIMPLE
Discretization schemes	
Gradient	Least squares cell based
Pressure	Second order
Momentum	QUICK
Turbulent kinetic energy	Second order upwind
Turbulent dissipation rate	Second order upwind
Transient formulation	Bounded second order implicit
Properties of the fluid	
Fluid	Water
Density [kg/m^3]	998.2
Dynamic viscosity [Pa $\cdot$ s]	0.001 003

The size of the time step for all calculated cases was set to 400 time steps per one period of function (1) which was controlling the velocity magnitude on the velocity inlet boundary condition. Volumetric efficiency was observed during the calculations. A calculation was considered converged when the volumetric efficiency became constant. The formula for volumetric efficiency is stated in the following section.

4. Evaluation of CFD calculations

All calculations were performed in order to obtain the volumetric efficiency of the pump. The volumetric efficiency was calculated by the following formula, which was used also by [5],

$$\eta_V = \frac{V_{DDD} - V_{SDS}}{V_{SDS} + V_{SSS}}, \tag{2}$$

where V_{DDD} is the volume displaced through the discharge piping at discharge, V_{SDS} is the volume sucked through the discharge piping at suction and V_{SSS} is the volume sucked through the suction piping at suction.

Mass flow rates at the discharge and suction pipings were recorded during the calculations (Fig. 4). The recorded curves of mass flow rates were integrated over time of suction and discharge to determine volumes for the volumetric efficiency formula.
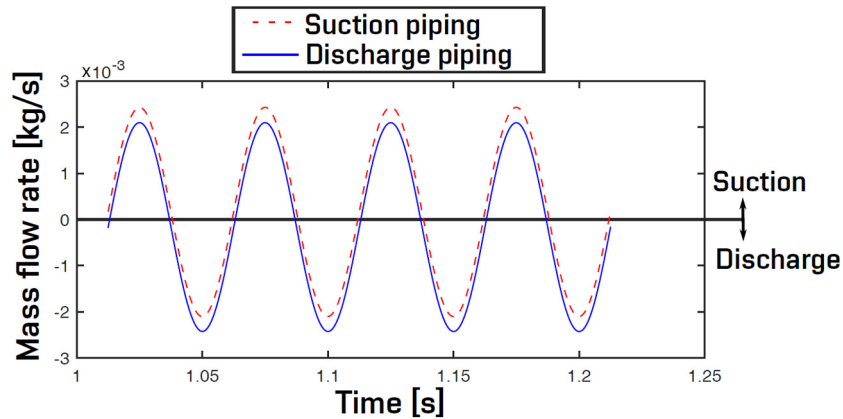
Fig. 4. Part of recorded mass flow rates of discharge and suction piping

The characteristics of the pump were obtained from CFD simulations. The first characteristics is the dependency of volumetric efficiency on the frequency of the piston motion. In this case, the volumetric efficiency was calculated for several values of the piston motion frequency. The value of amplitude was constant for all calculated frequencies. The settings for all cases are shown in Table 2.

Table 2. Values of frequency and amplitude used for the calculations

Amplitude [m]	0.012											
Frequency [Hz]	1	5	10	15	20	25	30	35	40	45	50	55	60

The calculated characteristic shown in Fig. 5 indicates that with increasing frequency, the volumetric efficiency is also increasing but from a certain frequency does not change much. The highest efficiency of 13.5% was achieved at the frequency of 60 Hz.
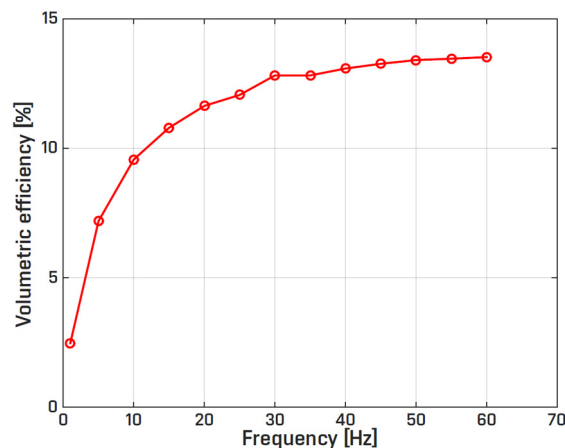
Fig. 5. Dependency of volumetric efficiency on frequency of the piston movement

The next obtained pump characteristic was the dependency of volumetric efficiency on the piston motion amplitude. In this case, the volumetric efficiency was calculated for several values of the amplitude. The frequency of the piston motion was constant for all calculated amplitudes. The settings for all the considered cases are shown in Table 3.

Table 3. Values of amplitude and frequency used for the calculations

Frequency [Hz]	40								
Amplitude [m]	0.006	0.009	0.012	0.015	0.018	0.021	0.024	0.027	0.030

The calculated characteristic in Fig. 6 shows that volumetric efficiency is increasing with increasing amplitude of the piston motion. The highest efficiency 22.6% was achieved at the amplitude of 0.03 m.
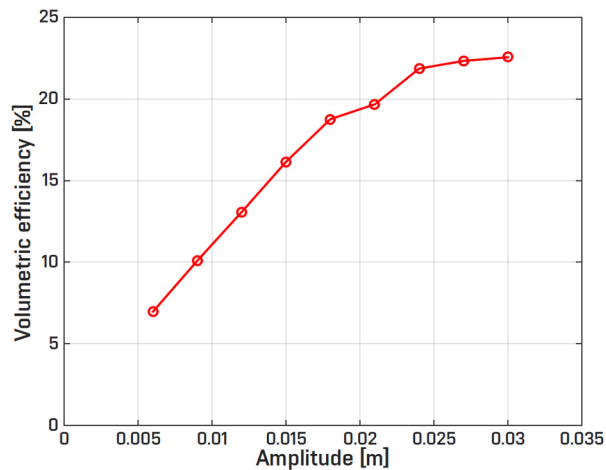
Fig. 6. Dependency of volumetric efficiency on amplitude of the piston movement

The last calculated characteristic of the pump is the dependency of the volumetric efficiency on the backpressure set on the pressure outlet of the discharge piping. In this case, the volumetric efficiency was computed for several values of backpressure. The characteristic was calculated for a constant value of amplitude and frequency. The settings for all cases are shown in Table 4.

Table 4. Values of backpressure, amplitude and frequency used for the calculations

Frequency [Hz]	40				
Amplitude [m]	0.021				
Backpressure [Pa]	0	500	1 000	1 500	2 000

The calculated characteristic (Fig. 7) shows that at backpressure value of 1 000 Pa, the pump has almost 0% volumetric efficiency. The pump has zero net flux at this value of backpressure.

Fig. 8 shows contours of vorticity at different operation modes of the pump. The discharge mode of the pump is shown in Fig. 8a. Here, it is possible to observe high vorticity in the suction diode. The high vorticity is filling the suction diode and preventing fluid going through it, while the vorticity in the discharge diode is much lower, so more fluid is diverted towards the discharge piping. Similar situation can be seen in Fig. 8c, where the suction mode of the pump
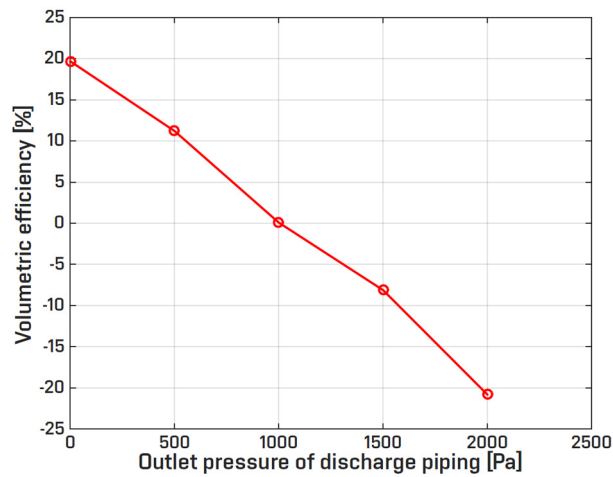
Fig. 7. Dependency of volumetric efficiency on the backpressure value

is shown. In this case, the vorticity is higher in the discharge diode and lower in the suction diode, so more fluid is sucked through the suction diode than through the discharge diode.

Analysis of Fig. 8 shows that the original intention was essentially achieved. Improvement of this state can be achieved by embedding an inlet cylinder inside the pump or by an oblique fluid entrance into the pump area.
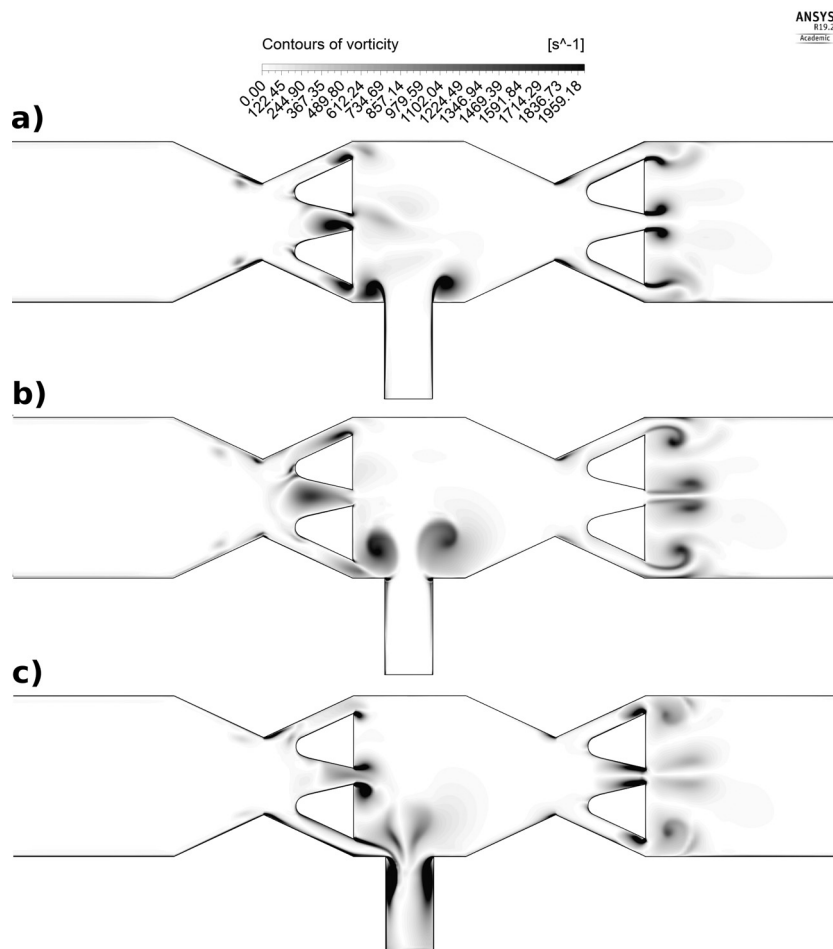
Fig. 8. Contours of vorticity at different operation modes of the pump for frequency 40 Hz and amplitude 0.03 m: a) discharge, $v_{\text{inlet}} = \max$; b) $v_{\text{inlet}} = 0$ m/s; c) suction, $v_{\text{inlet}} = \min$

5. Qualitative analysis of the dissipation function

To design an interior of a valveless pump, it is necessary to carry out a qualitative analysis of the dissipation function $D^T(\eta_T)$ which is caused by turbulent flow. The qualitative analysis was carried out depending on the operators $(\Omega = \text{rot } \mathbf{v})$ and $(\text{grad }|\mathbf{v}|^2)$.

The velocity vector is composed of a mean value $\mathbf{v}(\mathbf{x}, t)$ and a fluctuating part $\mathbf{u}'(\mathbf{x}, t)$

$$\mathbf{u}(\mathbf{x}, t) = \mathbf{v}(\mathbf{x}, t) + \mathbf{u}'(\mathbf{x}, t). \tag{3}$$

Then, it holds that

$$\mathbf{v}(\mathbf{x}, t) = \frac{1}{T} \int_{t-\frac{T}{2}}^{t+\frac{T}{2}} \mathbf{u}(\mathbf{x}, \tau) \, \mathrm{d}\tau \tag{4}$$

so the dissipation function can be defined by the following formula

$$2D^T = \int_V \Pi_{ijT} \frac{\partial v_i}{\partial x_j} \, \mathrm{d}V, \tag{5}$$

where

$$\Pi_{ijT} = 2\eta_T v_{ij} - \frac{2}{3}\delta_{ij}k. \tag{6}$$

Formula (5) was derived using the Gauss-Ostrogradsky theorem on a term of the RANS equations with the Reynolds stress tensor. The whole RANS equation was multiplied by a velocity vector:

$$\int_V \frac{\partial \Pi_{ijT}}{\partial x_j} v_i \, \mathrm{d}V = \int_S \Pi_{ijT} v_i n_j \, \mathrm{d}S - \int_V \Pi_{ijT} \frac{\partial v_i}{\partial x_j} \, \mathrm{d}V, \tag{7}$$

$$\int_V \frac{\partial \Pi_{ijT}}{\partial x_j} v_i \, \mathrm{d}V = 2 \int_S \left(\eta_T v_{ij} - \frac{1}{3}\delta_{ij}k \right) v_i n_j \, \mathrm{d}S - 2 \int_V \eta_T v_{ij} v_{ij} \, \mathrm{d}V. \tag{8}$$

Assuming that

$$v_{ij} v_{ij} > 0, \tag{9}$$

the mean value theorem for integrals can be used to simplify (8) as

$$\int_V \eta_T v_{ij} v_{ij} \, \mathrm{d}V = \hat{\eta}_T \int_V v_{ij} v_{ij} \, \mathrm{d}V =$$
$$= \hat{\eta}_T \int_V v_{ij} \frac{\partial v_i}{\partial x_j} \, \mathrm{d}V = -\hat{\eta}_T \int_V \frac{\partial v_{ij}}{\partial x_j} v_i \, \mathrm{d}V + \hat{\eta}_T \int_S v_{ij} v_i n_j \, \mathrm{d}S. \tag{10}$$

Then, it holds that

$$\int_V \frac{\partial \Pi_{ijT}}{\partial x_j} v_i \, \mathrm{d}V =$$
$$= 2 \left[\int_S \left(\eta_T v_{ij} - \frac{1}{3}\delta_{ij}k \right) v_i n_j \, \mathrm{d}S + \hat{\eta}_T \int_V \frac{\partial v_{ij}}{\partial x_j} v_i \, \mathrm{d}V - \hat{\eta}_T \int_S v_{ij} v_i n_j \, \mathrm{d}S \right]. \tag{11}$$

Following terms of equation (11), it can be expressed as

$$\int_V \frac{\partial v_{ij}}{\partial x_j} v_i \, \mathrm{d}V = -\frac{1}{2} \left[\int_S (\Omega \times \mathbf{v})\mathbf{n} \, \mathrm{d}S + \int_V \Omega \cdot \Omega \, \mathrm{d}V \right] \tag{12}$$

and

$$v_{ij}v_i n_j = \frac{1}{2}[(\boldsymbol{\Omega} \times \mathbf{v}) \cdot \mathbf{n} + \operatorname{grad} |\mathbf{v}|^2 \cdot \mathbf{n}]. \tag{13}$$

With the use of terms (12) and (13), equation (11) can be, after minor arrangements, written as

$$\int_V \frac{\partial \Pi_{ijT}}{\partial x_j} v_i \,\mathrm{d}V = \int_S \left\{ (\eta_T - 2\hat{\eta}_T)(\boldsymbol{\Omega} \times \mathbf{v}) \cdot \mathbf{n} + (\eta_T - \hat{\eta}_T)\operatorname{grad} |\mathbf{v}|^2 \cdot \mathbf{n} - \frac{2}{3}k)\mathbf{v} \right\} \mathrm{d}S -$$
$$-\hat{\eta}_T \int_V \boldsymbol{\Omega} \cdot \boldsymbol{\Omega} \,\mathrm{d}V. \tag{14}$$

From equations (5) and (7), the following formula for dissipation function can be derived

$$2D^T = \int_S \Pi_{ijT} v_i n_j \,\mathrm{d}S - \int_V \frac{\partial \Pi_{ij}^T}{\partial x_j} v_i \,\mathrm{d}V. \tag{15}$$

With the use of terms (6) and (13), the first term of formula (15) can be converted to

$$\int_S \Pi_{ijT} v_i n_j \,\mathrm{d}S = \int_S \eta_T [(\boldsymbol{\Omega} \times \mathbf{v}) \cdot \mathbf{n} + \operatorname{grad} |\mathbf{v}|^2 \cdot \mathbf{n}] \,\mathrm{d}S - \int_S \frac{2}{3}k\mathbf{v} \cdot \mathbf{n} \,\mathrm{d}S. \tag{16}$$

The final formula for dissipation function is obtained by substituting terms (14) and (16) into formula (15). After simplification, the formula for dissipation function can be written as

$$2D^T = \hat{\eta}_T \left[\int_V \boldsymbol{\Omega} \cdot \boldsymbol{\Omega} \,\mathrm{d}V + \int_S \operatorname{grad} |\mathbf{v}|^2 \cdot \mathbf{n} \,\mathrm{d}S + 2 \int_S (\boldsymbol{\Omega} \times \mathbf{v}) \cdot \mathbf{n} \,\mathrm{d}S \right]. \tag{17}$$

The dissipation function is obviously dependent on the mean value of turbulent viscosity, however, its influence will not play a major role in areas near fluidic diodes. Similar point of view is also taken on the influence of the term with the volumetric integral. The last two terms of dissipation function will have a dominant influence on the function of fluidic diodes when the fluid will be entering or leaving the area of the diodes. The vector product of $\boldsymbol{\Omega}$ and $\mathbf{v}$ is related to the creation of spiral vortices, which are defined by the following equation

$$\boldsymbol{\Omega} \times \mathbf{v} = 0. \tag{18}$$

In that case, fluid will flow through the diode with a strong rotational component, which can be used for increasing as well as decreasing flow rate through the diode.

The essential influence on the performance of diodes has the integral

$$\int_S \operatorname{grad} |\mathbf{v}|^2 \cdot \mathbf{n} \,\mathrm{d}S. \tag{19}$$

Its value can be easily influenced by various designs of both the inlet and the outlet of a diode.

6. Conclusions

A new design of a valveless piston pump for macro scale was presented. Characteristics of the pump were computed using CFD simulations in ANSYS Fluent software. The dependence of volumetric efficiency on the amplitude and frequency of piston movement and backpressure was investigated on a simplified 2D geometry model of the pump. Piston motion was simulated

by a time-dependent velocity inlet boundary condition placed at the end of the cylinder. The pump achieved volumetric efficiency of 22.6% at frequency 40 Hz and amplitude 0.03 m. The dependence of volumetric efficiency on the value of backpressure was examined at frequency 40 Hz and amplitude 0.021 m. With increasing value of backpressure, the volumetric efficiency was rapidly decreasing. At value of 1 000 Pa of backpressure the pump had 0% efficiency.

Qualitative analysis of the dissipation function was carried out in order to better understand the principle of the pump. The result of the analysis shows that the dissipation can be significantly increased/decreased if spiral vortices are created near fluidic diodes. This analysis will be used in future research to increase the pump efficiency and to raise the value of backpressure applied on discharge pumping.

Future work will also focus on further CFD simulations with complete 3D geometry with piston motion simulated by a dynamic mesh. This approach should provide more accurate results.

Acknowledgements

References

[1] Foster, F., Bardell, R., Afromowitz, M., Sharma, N., Blanchard, A., Design, fabrication and testing of fixed-valve micro-pumps, Proceedings of the ASME Fluids Engineering Division 234 (1995) 39–44.

[2] Gamboa, A., Morris, C., Foster, F., Improvements in fixed-valve micropump performance through shape optimization of valves, Journal of Fluids Engineering 127 (2) (2005) 339–346. https://doi.org/10.1115/1.1891151

[3] Gerlach, T., A new micropump principle of the reciprocating type using pyramidic micro flowchannels as passive valves, Journal of Micromechanics and Microengineering 5 (2) (1995) 199–201. https://doi.org/10.1088/0960-1317/5/2/039

[4] He, X., Zhu, J., Zhang, X., Xu, L., Yang, S., The analysis of internal transient flow and the performance of valveless piezoelectric micropumps with planar diffuser/nozzles elements, Microsystem Technologies 23 (1) (2017) 23–37. https://doi.org/10.1007/s00542-015-2695-0

[5] Kordík, J., Trávníček, Z., Novel fluidic diode for hybrid synthetic jet actuator, Journal of Fluids Engineering 135 (10) (2013) 1–7. https://doi.org/10.1115/1.4024679

[6] Kulkarni, A., Ranade, V., Rajeev, R., Koganti, S., CFD simulation of flow in vortex diodes, AIChE Journal 54 (5) (2008) 1139-1152. https://doi.org/10.1002/aic.11439

[7] NuViesion Engineering, Vortex diode pumps: No moving part pumping systems, product profile, 2011.

[8] Olsson, A., Stemme, G., Stemme, E., A valve-less planar fluid pump with two pump chambers, Sensors & Actuators A: Physical 47 (1) (1995) 549–556. https://doi.org/10.1016/0924-4247(94)00960-P

[9] Ottesen, J. T., Valveless pumping in a fluid-filled closed elastic tube-system: One-dimensional theory with experimental validation, Journal of Mathematical Biology 46 (4) (2003) 309–332. https://doi.org/10.1007/s00285-002-0179-1

[10] Shin, S., Chang, C., Sung, H., Simulation of a valveless pump with an elastic tube, International Journal of Heat and Fluid Flow 38 (2012) 13–23. https://doi.org/10.1016/j.ijheatfluidflow.2012.08.003

[11] Stemme, E., Stemme, G., A valveless diffuser/nozzle-based fluid pump, Sensors & Actuators A: Physical 39 (2) (1993) 159–167. https://doi.org/10.1016/0924-4247(93)80213-Z

[12] Tesař, V., Pump for extremely dangerous liquids, Chemical Engineering Research and Design 89 (7) (2011) 940–956. https://doi.org/10.1016/j.cherd.2010.11.022

[13] Tesař, V., Safe pumping of hazardous liquids-A survey of no-moving-part pump principles, Chemical Engineering Journal 168 (1) (2011) 23–34. https://doi.org/10.1016/j.cej.2011.01.046

[14] Tesla, N., Valvular conduit, U.S. Patent No. 1, 329, 559, 1920.

[15] Wada, T., Shimizu, A., Takagi, M., Studies on the efficiency of fluidic pump with vortex diodes, Transactions of the Society of Instrument and Control Engineers 20 (5) (1984) 442–446. https://doi.org/10.9746/sicetr1965.20.442

[16] Wen, C., Yeh, S., Leong, K., Kuo, W., Lin, H., Application of a valveless impedance pump in a liquid cooling system, IEEE Transactions on Components, Packaging and Manufacturing Technology 3 (5) (2013) 783–791. https://doi.org/10.1109/TCPMT.2012.2230298